Determination of ψ Torsion Angle Restraints from $^3J(C_\alpha,C_\alpha)$ and $^3J(C_\alpha,H^N)$ Coupling Constants in Proteins

Mirko Hennig,[†,⊥] Wolfgang Bermel,[‡] Harald Schwalbe,*[,†,§] and Christian Griesinger*[,†,||]

Contribution from the Institut für Organische Chemie, Universität Frankfurt, Marie-Curie Strasse 11, D-60439 Frankfurt/Main, Germany, Bruker Analytik GmbH, Silberstreifen, D-76287 Rheinstetten, Germany, Massachusetts Institute of Technology, Department of Chemistry, Francis Bitter Magnet Laboratory, 170 Albany Street, Building NW14, Cambridge, Massachusetts 02139, and Max Planck Institut für Biophysikalische Chemie, Am Faßberg, D-37077 Göttingen, Germany

Received August 9, 1999. Revised Manuscript Received March 28, 2000

Abstract: Homonuclear $^3J(C_\alpha,C_\alpha)$ and heteronuclear $^3J(C_\alpha,H^N)$ coupling constants have been determined in the protein ubiquitin. Despite the fact that all amide bonds in ubiquitin have a *trans* conformation, considerable spread in the size of the coupling constants can be observed. The $^3J(C_\alpha,H^N)$ coupling constants vary from 0.0 to 1.0 Hz, and the $^3J(C_\alpha,C_\alpha)$ coupling constants that could be determined vary from 1.1 to 2.2 Hz. Interpretation of the coupling constants reveals a non-Karplus-type dependence and suggests that vicinal homonuclear $^3J(C_\alpha,C_\alpha)$ and heteronuclear $^3J(C_\alpha,H^N)$ depend on the ψ_{i-1} torsion angle. The proposed sensitive E.COSY-type HNCO[C_α] experiment for the measurement of vicinal $^3J(C_\alpha,H^N)$ coupling constants can be used in protonated and deuterated proteins, and the quantitative *J* correlation experiment HN(COCA)CA can be carried out on perdeuterated proteins for the measurement of $^3J(C_\alpha,C_\alpha)$ that provide unique torsion angle information in these proton sparse proteins.

Introduction

A large number of different experiments for the determination of vicinal coupling constants have been developed to characterize backbone and side chain conformations of proteins by NMR spectroscopy. For the backbone torsion angle ϕ for example, methods are available to determine all six different vicinal coupling constants. The quantification of the experimental coupling constants relies on Karplus relationships,[1] $^3J = A\cos^2\phi + B\cos\phi + C$. Integrating torsion angle restraints derived from vicinal coupling constants has become a routine step in three-dimensional structure determination of proteins by NMR.

In contrast, the angle ψ is characterized only by three vicinal coupling constants, $^3J(N,N)$, $^3J(N,C_\beta)$ and $^3J(N,H_\alpha)$. A comparable analysis of the torsion angle ψ is hampered by the rather small values of vicinal couplings observed whenever a ^{15}N nucleus with a low gyromagnetic ratio is one of the coupling partners.

Our investigations reported here were stimulated by observation of varying $^3J(C_\alpha,C_\alpha)$ couplings in spectra originally designed for the determination of $^3J(C_\alpha,C_\delta)$ coupling constants. $^3J(C_\alpha,C_\alpha)$ coupling constants should to a first approximation only depend on the torsion angle ω. The variation was unexpected since in proteins, the torsion angle ω varies in very narrow ranges due to the planarity of the peptide bond (C′−N) which is maintained by a rotational barrier of about 80.0 kJ mol^{-1}.[2,3] The peptide bond in proteins occupies predominantly the *trans* conformation. Out of 72,567 ω torsion angles in a set of 291 non-redundant protein crystal structures with a resolution better than 2.0 Å taken from the Brookhaven protein database only 232 (0.32%) were found to be in the disfavored *cis* conformation.[4]

Further statistical analysis of protein crystal structures revealed mean angles of $\omega = 179.8°$ (±0°) for the *trans* conformer and $\omega = -2.9°$ (±24.1°) for the *cis* conformer, respectively.[5] A similar statistical study was carried out by MacArthur and Thornton using the Cambridge Structural Database of small molecules.[6] Their analysis of a dataset containing 492 *trans* peptide bonds in small peptides with their respective structures determined mostly by X-ray crystallography under favorable conditions to atomic resolution revealed an almost identical mean angle of $\omega = 179.7°$ (±5.9°). In addition, NMR studies carried out for the protein ubiquitin using six different ϕ related vicinal coupling constants provide further evidence for small average deviations from planarity of less than 8° between planes defined by atoms $^{13}C'_{i-1}$,$^{15}N_i$,$^{13}C_{\alpha i}$ and $^1H^N_i$,$^{15}N_i$,$^{13}C_{\alpha i}$.[7] The analysis of $^1J(H^N,N)$ coupling constant values determined for ubiquitin indicate an out-of-$^{13}C'_{i-1}$,$^{15}N_i$,$^{13}C_{\alpha i}$-plane angle for the amide proton of no more than 5°.[8] This small degree of nonplanarity expressed by the torsion angle ω was

* Authors for correspondence. E-mail: cigr@org.chemie.uni-frankfurt.de; schwalbe@ccnmr.mit.edu.
† Universität Frankfurt.
‡ Bruker Analytik GmbH.
§ Massachusetts Institute of Technology.
|| Max Planck Institut für Biophysikalische Chemie.
⊥ Present address: Department of Molecular Biology & The Skaggs Institute of Chemical Biology, The Scripps Research Institute, MB 33, 10550 North Torrey Pines Road, La Jolla, CA 92037.

(1) Karplus, M. *J. Chem. Phys.* **1959**, *30*, 11−15.
(2) Ramachandran, G. N.; Sasisekharan, V. *Adv. Protein Chem.* **1968**, *23*, 283−438.
(3) LaPlanche, L. A.; Rogers, M. T. *J. Am. Chem. Soc.* **1964**, *86*, 337.
(4) Weiss, M. S.; Jabs, A.; Hilgenfeld, R. *Nat. Struct. Biol.* **1998**, *5*, 676.
(5) Stewart, D. E.; Sarkar, A.; Wampler, J. E. *J. Mol. Biol.* **1990**, *214*, 253−260.
(6) MacArthur, M. W.; Thornton, J. M. *J. Mol. Biol.* **1996**, *264*, 1180−1195.
(7) Hu, J.-S.; Bax, A. *J. Am. Chem. Soc.* **1997**, *119*, 6360−6368.
(8) Tjandra, N.; Grzesiek, S.; Bax, A. *J. Am. Chem. Soc.* **1996**, *118*, 6264−6272.

10.1021/ja9928834 CCC: $19.00
Published on Web 06/14/2000

confirmed for ubiquitin from molecular dynamic (MD) simulations.[9] Consequently, detectable variations in associated $^3J(C_\alpha,C_\alpha)$ and $^3J(C_\alpha,H^N)$ coupling constant values that were determined in the present study should be of vanishing magnitude for the individual *trans* and *cis* conformations, but methods should be suitable for the differentiation of both conformers.

While $^3J(C_\alpha,H^N)$ coupling constants are readily determined in protonated and deuterated proteins, $^3J(C_\alpha,C_\alpha)$ can only be determined in proteins with favorable $^{13}C_\alpha$ relaxation properties. It is shown, however, that the size of $^3J(C_\alpha,C_\alpha)$ and $^3J(C_\alpha,H^N)$ coupling constants depends on variation in backbone angle ψ and can be used to differentiate between values of ψ typical for α-helical and β-sheet structures.

Results and Discussion

The experimental schemes, which we refer to as HN(COCA)CA and HNCO[C_α] are of the quantitative *J*-correlation[10] and of the E.COSY type,[11] respectively. The first pulse scheme is closely related to the HN(COCA)C_{ali}[12] previously published and relies on a rather long transfer delay with $^{13}C_\alpha$ nuclei being transverse thus requiring ^2H substitution for the investigation of proteins. The quantitative *J*-correlation experiment used here employs a modified homonuclear ^{13}C decoupling scheme previously publishished by Kupče and Wagner.[13]

The second experiment is derived from a conventional and sensitive HNCO experiment,[14] the E.COSY requirement can easily be fulfilled by leaving the $^{13}C_\alpha$ nuclei untouched throughout the sequence. The measured $^3J(C_\alpha,C_\alpha)$ and $^3J(C_\alpha,H^N)$ coupling constant values in human ubiquitin show a considerable spread along the sequence despite the fact that all 76 peptide bonds taken from the crystal structure are in the *trans* conformation.[15] Ubiquitin is among the best available test systems because a large consistent set of structural parameters derived from different methods such as X-ray crystallography,[15] heteronuclear NMR spectroscopy[7,8] as well as MD computer simulations[9] is available for comparison. The observable homonuclear $^3J(C_\alpha,C_\alpha)$ coupling constants for ubiquitin fall in the range from 2.2 to 1.1 Hz with a mean value of 1.6 (±0.2) Hz. For a number of residues located in the regions of ubiquitin with helical conformations, the coupling constant is apparently too small to be observed. The heteronuclear $^3J(C_\alpha,H^N)$ coupling constant values vary between 0.0 and 1.0 Hz with a mean value of 0.5 (±0.3) Hz.

These significant variations cannot be explained on the basis of a Karplus-type dependence on the backbone torsion angle ω as large differences in measured $^3J(C_\alpha,C_\alpha)$ and $^3J(C_\alpha,H^N)$ coupling constant values are observed for residues with very similar backbone angles ω.

Considering the atoms $^{13}C_{\alpha i-1}$,$^{13}C'_{i-1}$,$^{15}N_i$,$^{13}C_{\alpha i}$, the geometry and the electron distribution of an adjacent $^{13}C_\alpha$ atom of residue $i-1$ changes dramatically upon rotating the torsion angle ψ_{i-1} from $\psi_{i-1} = -39.8°$ typical for an α-helical secondary structure to $\psi_{i-1} = 123.0$ typical for a β-sheet secondary structure, whereas the geometry of the $^{13}C_\alpha$ atom of residue *i* is far less sensitive to variations of the torsion angle ϕ_i associated with the regular secondary structure elements, $\phi_i = -64.7°$ (α-helix) and $\phi_i = -112.6°$ (β-sheet).[16] In contrast to what one expects from a Karplus-type dependence on the backbone torsion angle ω, the experimentally derived values for the respective vicinal couplings cluster in distinct regions, reflecting a strong dependence on the neighboring backbone torsion angle ψ. Both vicinal coupling constants under investigation involving the $^{13}C_\alpha$ nuclei, $^3J(C_\alpha,C_\alpha)$ and $^3J(C_\alpha,H^N)$, are well suited to qualitatively define the ψ torsion angle.

Experimental Section

A sample of commercially available uniformly ^2H,^{13}C,^{15}N-labeled human ubiquitin (VLI Research, Malvern, PA) was used without further purification. Ten milligrams of the protein were dissolved in 500 μL of 95% H_2O, 5% D_2O containing 30 mM sodium acetate buffer, pH 4.7. All spectra were recorded on a four-channel BRUKER DRX600 spectrometer equipped with an actively shielded *z*-gradient triple-resonance probe at a temperature of 303 K. Sequential assignments of the ^1H, ^{13}C, and ^{15}N chemical shifts of perdeuterated ubiquitin were verified using through-bond heteronuclear correlations: CT-HNCA[17] and HN(CA)CB.[18]

All experiments involving $^1H^N$ detection utilized pulsed field gradients for coherence order selective coherence transfer,[19,20] making use of an enhanced sensitivity approach[21] with minimal water saturation.[22,23] Quadrature detection in all indirect carbon ω_2 dimensions was achieved via the States-TPPI method.[24] The HN(COCA)CA and the HNCO[C_α] data sets both compromised 24 complex points with an acquisition time of 14.7 ms for ^{15}N (ω_1) and 1024 complex points with an acquisition time of 140.4 ms for $^1H^N$ (ω_3) at a ^1H frequency of 600 MHz. The following numbers of complex points and acquisition times were employed in the experiments for carbon evolution times used in this study: HNCO[C_α],$^{13}C'$ (ω_2) 64, 36.1 ms (four transients) and HN(COCA)CA,$^{13}C_\alpha$ (ω_2) 48, 14.7 ms (eight transients). A repetition delay between transients of 2.0 s was used. The resulting total measuring times were 14.6 and 22 h for the HNCO[C_α] and the HN(COCA)CA experiment, respectively.

Spectra were processed and analyzed using the program Felix 95.0 (Biosym/MSI, San Diego, CA). A solvent suppression filter was used in the ω_3 dimension to eliminate distortions from residual water[25] prior to apodization with a 72° shifted squared sinebell window function. Data sets were zerofilled twice and Fourier transformed, retaining only the $^1H^N$ region of the spectra. For constant time ^{15}N evolution times (ω_1), mirror image linear prediction[26] was used to double the time domain signal prior to apodization with a 72° shifted squared sinebell window function. The ω_2 dimensions were zerofilled and apodized with a 72° shifted squared sinebell window function prior to Fourier transformation. The absorptive part of the final 3D matrixes consists of 1024 × 256 × 128 for the HNCO[C_α] experiment and of 1024 × 128 × 128 for the HN(COCA)CA experiment, respectively.

(9) Lienin, S. F.; Bremi, T.; Brutscher, B.; Brüschweiler, R.; Ernst, R. R. *J. Am. Chem. Soc.* **1998**, *120*, 9870−9879.
(10) Bax, A.; Vuister, G. W.; Grzesiek, S.; Delaglio, F.; Wang, A. C.; Tschudin, R.; Zhu, G. *Methods Enzymol.* **1994**, *239*, 79−105.
(11) Griesinger, C.; Sørensen, O. W.; Ernst, R. R. *J. Am. Chem. Soc.* **1985**, *107*, 6394−6396.
(12) Hennig, M.; Ott, D.; Schulte, P.; Löwe, R.; Krebs, J.; Vorherr, T.; Bermel, W.; Schwalbe, H.; Griesinger, C. *J. Am. Chem. Soc.* **1997**, *119*, 5055−5056.
(13) Kupče, Ē.; Wagner, G. *J. Magn. Reson., Ser. B* **1996**, *110*, 309−312.
(14) Ikura, M.; Kay, L. E.; Bax, A. *Biochemistry* **1990**, *29*, 4659−4667.
(15) Vijay-Kumar, S.; Bugg, C. E.; Cook, W. J. *J. Mol. Biol.* **1987**, *194*, 531−544.
(16) Smith, L. J.; Bolin, K. A.; Schwalbe, H.; MacArthur, M. W.; Thornton, J. M.; Dobson, C. M. *J. Mol. Biol.* **1996**, *255*, 494−506.
(17) Yamazaki, T.; Lee, W.; Revington, M.; Matiello, D. L.; Dahlquist, F. W.; Arrowsmith, C. H.; Kay, L. E. *J. Am. Chem. Soc.* **1994**, *116*, 6464−6465.
(18) Yamazaki, T.; Lee, W.; Arrowsmith, C. H.; Muhandiram, R.; Kay, L. E. *J. Am. Chem. Soc.* **1994**, *116*, 11655−11666.
(19) Kay, L. E.; Keifer, P.; Saarinen, T. *J. Am. Chem. Soc.* **1992**, *114*, 10663−10665.
(20) Schleucher, J.; Sattler, M.; Griesinger, C. *Angew. Chem., Int. Ed. Engl.* **1993**, *32*, 1489−1491.
(21) Palmer, A. G., III; Cavanagh, J.; Wright, P. E.; Rance, M. *J. Magn. Reson.* **1991**, *91*, 429−436.
(22) Grzesiek, S.; Bax, A. *J. Am. Chem. Soc.* **1993**, *115*, 12593−12594.
(23) Kay, L. E.; Xu, G. Y.; Yamazaki, T. *J. Magn. Reson., Ser. A* **1994**, *109*, 129−133.
(24) Marion, D.; Ikura, M.; Tschudin, R.; Bax, A. *J. Magn. Reson.* **1989**, *85*, 393−399.
(25) Marion, D.; Ikura, M.; Bax, A. *J. Magn. Reson.* **1989**, *84*, 425−430.
(26) Zhu, G.; Bax, A. *J. Magn. Reson.* **1990**, *90*, 405−410.

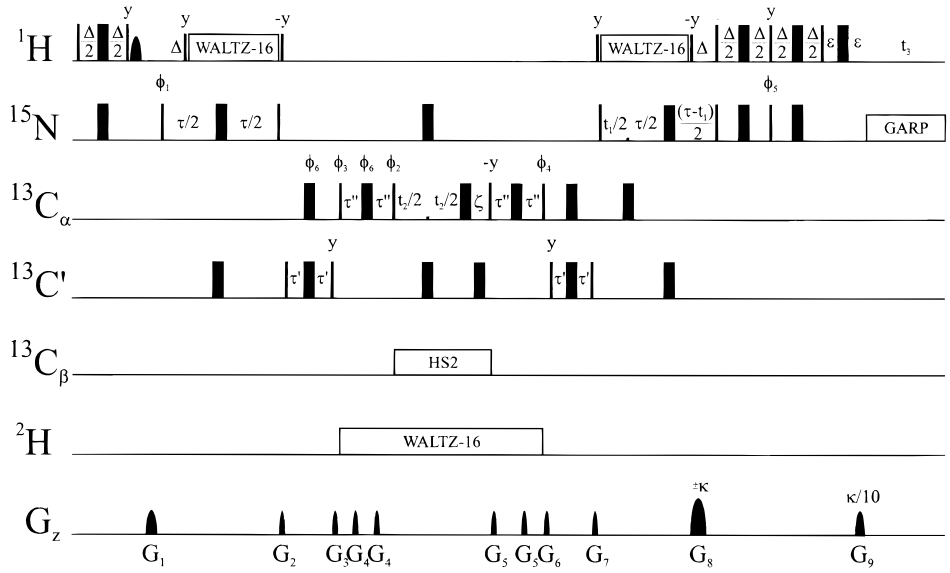

Figure 1. Pulse sequence of the quantitative HN(COCA)CA experiment. Carrier positions in the present work were 119.9 ppm for ^{15}N, 175.5 ppm for ^{13}C′, 55.5 ppm for $^{13}C_\alpha$, 4.5 ppm for ^{2}H, and 4.7 ppm for $^1H^N$, respectively. All ^{1}H pulses were given on resonance on the water signal. Water-selective pulses were 2 ms rectangular pulses (125 Hz),$^1H^N$ decoupling was achieved using a 3.5 kHz WALTZ-16[58] decoupling field with 3.5 kHz flanking pulses on either side of the decoupling field, while high power proton pulses were applied with a field strength of 36 kHz.^{15}N decoupling during acquisition employed a 1.1 kHz GARP[59] field, while high power ^{15}N pulses were applied with a field strength of 7.3 kHz. ^{2}H decoupling during t_2 is achieved with WALTZ-16 at a field of 926 Hz. All ^{13}C′ excitation pulses were G4 Gaussian cascades[28] with a duration of 409.6 μs. Every second G4 was applied time-reversed. All $^{13}C_\alpha$ excitation pulses were rectangular and applied with $\gamma B_1/2\pi = 4675$ Hz. Off-resonant selective G3 inversion pulses of durations 512 and 256 μs during $^{13}C_\alpha-^{13}$C′ INEPT transfers were implemented as phase modulated pulses.[60] The carbon carrier frequency was 175.5 ppm for ^{13}C′. It was changed during the pulse sequence to 55.5 ppm prior to the pulse labeled with phase ϕ_3 and returned to 175.5 ppm after the pulse labeled with phase ϕ_4. Bandselective $^{13}C_\alpha$ inversion pulses in the middle of the de- and refocusing delays τ'' and during t_2 had the Q3 shape and a length of 1 ms.[28] Asynchronous homonuclear $^{13}C_\beta$ decoupling with $(\gamma B_1/2\pi)^{max} = 1691.5$ Hz uses HS2 adiabatic pulses[36,37] of duration 4 ms expanded according to a nested combination of the (0°, 60°, 150°, 60°, 0°) cycle proposed by Tycko et al.[61] and the MLEV-4 (0°, 0°, 180°, 180°) scheme[62] leading to a 20-step supercycle. See text for further details. Phase cycling: $\phi_1 = x, -x$, $\phi_2 = 4(y), 4(-y)$, $\phi_3 = 2(x), 2(-x)$, $\phi_4 = x$, $\phi_5 = -y$, $\phi_6 = x$, receiver $= x, -x, -x, -x$. Quadrature detection in the t_2 dimension was obtained by altering ϕ_2, ϕ_3, and ϕ_6 according to States-TPPI. For each t_1 value, echo- and antiecho coherences were obtained by recording data sets where the phase ϕ_5 and gradient G_8 were inverted. Delay durations: $\Delta = 5.5$ ms, $\tau = 25.6$ ms, $\tau' = 4.55$ ms, $\tau'' = 28.2$ ms, $\zeta = t_2(0)$ and $\epsilon = 1.2$ ms. Sine-shaped gradient durations and amplitudes were: G_1 2 ms (25 G/cm); G_2 1 ms (6.5 G/cm); G_3 0.75 ms (11.5 G/cm); G_4 0.5 ms (5.5 G/cm); G_5 0.5 ms (4 G/cm); G_6 0.5 ms (2.5 G/cm); G_7 0.75 ms (8.5 G/cm); G_8 1 ms (40 G/cm); G_9 1 ms (4.05 G/cm).

Determination of Homonuclear $^3J(C_\alpha,C_\alpha)$ Coupling Constants. The pulse sequence for the determination of homonuclear $^3J(C_\alpha,C_\alpha)$ coupling constants is similar to the quantitative *J*-correlation HN(COCA)C_{ali} scheme previously published for the determination of $^3J(C_\alpha,C_\delta)$ coupling constants related to the side-chain angle χ_2.[12] The employed HN(COCA)CA sequence is based on a regular "out and back" HN(CO)CA experiment combined with homonuclear $^{13}C_\beta$ decoupling and ^{2}H decoupling. The magnetization transfer has been discussed in detail in the literature.[27] We will therefore focus on the experimental aspects important for the quantification of the homonuclear $^3J(C_\alpha,C_\alpha)$ coupling constants and the corresponding pulse sequence elements. Figure 1 depicts the pulse scheme for the determination of $^3J(C_\alpha,C_\alpha)$ couplings. The created transverse $^{13}C_\alpha$ magnetization defocuses with respect to its long-range $^{13}C_\alpha$ coupling partners during a period $2\tau'' = 57.2$ ms ($\sim 2/^1J(C,C)$). The fraction of magnetization giving rise to the reference peak intensity is proportional to $\cos(2\pi J_{C\alpha iC\alpha i\pm1}\tau'')\Pi_k\cos(2\pi J_{C\alpha iCk}\tau'')$, $k \neq C_{\alpha i},C_{\alpha i\pm1}$, while the transfer efficiency for the cross-peak intensity is proportional to $\sin(2\pi J_{C\alpha iC\alpha i\pm1}\tau'')\Pi_k\cos(2\pi J_{C\alpha iCk}\tau'')$. The combined effect of the chosen defocusing delay duration and the $^{13}C_\alpha$ band selective refocusing Q3[28] pulse of duration 1 ms in the middle of the delay $2\tau''$ ensure the minimization of unwanted $C_{\alpha i}$-C_k correlations. After chemical shift evolution of the $^{13}C_\alpha$ magnetization during t_2, the same fractions are refocused following the reverse pathway. Thus, the ratio of the transfer amplitudes of the reference and the cross-peak intensity equals $-\tan^2(2\pi J_{C\alpha iC\alpha i\pm1}\tau'')$. Because the line shapes of the cross and the reference signal in ω_1 (^{15}N) and ω_3 ($^1H^N$) are the same and the line shape in the ω_2 ($^{13}C_\alpha$) dimension is limited by digitization since t_2^{max} is kept short compared to the relevant relaxation times, values of $^3J(C_\alpha,C_\alpha)$ can be derived from the intensity ratio, $I^{cross}/I^{ref} = -\tan^2(2\pi J_{C\alpha iC\alpha i\pm1}\tau'')$.

Relaxation Effects. For reliable quantification of coupling constants from quantitative *J*-experiments, in-phase and antiphase coherences, giving rise to the reference and the cross-peak intensity, respectively, have to relax at identical rates which is usually not valid.[29,30] Differential relaxation of $^{13}C_\alpha$ in-phase and antiphase magnetization results in a decrease of the apparent coupling constant,[31] considering finite $^{13}C_\alpha$ T_1 relaxation times compared to the lengthy de- and refocusing delays $2\tau''$. Because no T_1 values for deuterated $^{13}C_\alpha$ have been reported, no correction is made. However, Wand et al. studied the dynamical behavior of $^{13}C_\alpha$ carbon atoms in a randomly and fractionally ^{13}C enriched sample of human ubiquitin.[32] They reported extensive variations for the longitudinal T_1 times of protonated $^{13}C_\alpha$ spins in the range between 0.25 and 0.50 s at a carbon frequency of 125 MHz. Correcting for this finite $^{13}C_\alpha$ T_1 relaxation rate following Hu and Bax would increase apparent $^3J(C_\alpha,C_\alpha)$ coupling constant values by ~10% for $^{13}C_\alpha$ $T_1 = 0.25$ s.[7] Because of the approximately 6.5-fold lower gyromagnetic ratio of ^{2}H compared to that of ^{1}H, dipolar contributions to the longitudinal relaxation times T_1 scale as a result of the substitution of ^{1}H by ^{2}H according to $T_1(^{13}C_\alpha,H_\alpha)/T_1(^{13}C_\alpha,D_\alpha) \approx \gamma_C^2\gamma_H^2 I(I+1)/$

(27) Matsuo, H.; Kupèe, Ç.; Li, H.; Wagner, G. *J. Magn. Reson., Ser. B* **1996**, *113*, 91−96.
(28) Emsley, L.; Bodenhausen, G. J. *J. Magn. Reson.* **1992**, *97*, 135−148.
(29) Harbison, G. S. *J. Am. Chem. Soc.* **1993**, *115*, 3026−3027.
(30) Norwood, T. J.; Jones, K. *J. Magn. Reson. Ser. A* **1993**, *104*, 106−110.
(31) Rexroth, A.; Schmidt, P.; Szalma, S.; Geppert, T.; Schwalbe, H.; Griesinger, C. *J. Am. Chem. Soc.* **1995**, *117*, 10389−10390.
(32) Wand, A. J.; Urbauer, J. L.; McEvoy, R. P.; Bieber, R. J. *Biochemistry* **1996**, *35*, 6116−6125.

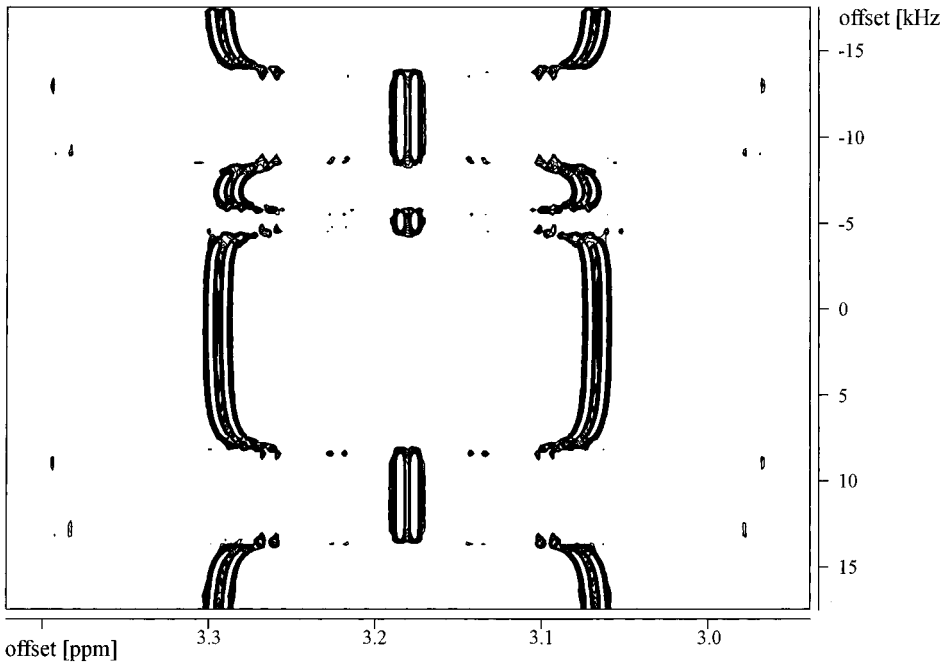

Figure 2. Experimental performance of the HS2 homonuclear decoupling of ^{13}C while observing proton magnetization of a labeled ^{13}C-MeOH sample in DMSO. The pseudo 2D profile is recorded as a function of the offset swept from −17.5 kHz to 17.5 kHz in increments of 250 Hz. The decoupling RF amplitude is $(\gamma B_1/2\pi)^{max} = 6720$ Hz, the basic HS2 inversion pulses of duration 4 ms are expanded with a nested combination of the (0°, 60°, 150°, 60°, 0°) cycle proposed by Tycko et al.[61] and the MLEV-4 (0°, 0°, 180°, 180°) scheme[62] leading to a 20-step supercycle.

$[\gamma_C^2\gamma_D^2 S(S+1)] \approx 16$. Contributions from dipolar coupled adjacent ^{13}C and ^{15}N spins and contributions due to the $^{13}C_\alpha$ CSA, all of which are of considerably smaller magnitude, remain unchanged. ^2H decoupling throughout pulse sequence elements where $^{13}C_\alpha$ magnetization is transverse ensures suppression of scalar relaxation of the second kind, consequently, the effect of $^{13}C_\alpha$ spin flip rates leads to negligible underestimation of the true vicinal $^3J(C_\alpha,C_\alpha)$ coupling constants. All reported vicinal coupling constant values were not corrected for $^{13}C_\alpha$ spin flips.

Homonuclear $^{13}C_\beta$ Decoupling. The homonuclear $^{13}C_\beta$ decoupling during the $^{13}C_\alpha$ chemical shift evolution (t_2) pioneered by Wagner and co-workers[33] turned out to be essential for the quantification of reliable $^3J(C_\alpha,C_\alpha)$ coupling constant values. Prior attempts assuming uniform values of one-bond $^1J(C_\alpha,C_\beta)$ coupling constants and recording the $^{13}C_\alpha$ chemical shifts in a constant time manner choosing a CT-delay of $1/^1J(C_\alpha,C_\beta)$ did not allow the quantification of $^3J(C_\alpha,C_\alpha)$ coupling constants. A number of the backbone $^{13}C_\alpha$ chemical shifts are sufficiently resolved to measure the $^3J(C_\alpha,C_\alpha)$ coupling constant values twice, once starting from $^{13}C_{\alpha i}$ and detection of the cross-peak intensity at the frequency of $^{13}C_{\alpha i-1}$, and once vice versa. When using a constant time approach to measure the coupling constants, the pairwise root-mean-square (rms) difference between these measurements were unusually high which can mainly be attributed to the small variations in one-bond $^1J(C_\alpha,C_\beta)$ coupling constants of adjacent residues. This results in differential attenuation of reference and cross-peak intensities. Utilizing a modified homonuclear $^{13}C_\beta$ decoupling scheme during the t_2 evolution period, the pairwise rms difference drops significantly to values comparable to measurements of homonuclear $^3J(C',C')$ coupling constants (see Supporting Information).[34]

Homonuclear $^{13}C_\beta$ decoupling allowed incrementation of the indirect $^{13}C_\alpha$ dimension (ω_2) in a nonconstant time manner, thereby increasing both the sensitivity of the HN(COCA)CA sequence and eliminating the differential attenuation of reference and cross-peak intensities caused by nonuniform $^1J(C_\alpha,C_\beta)$ coupling constants. It should be noted that glycine $^{13}C_\alpha$ resonances are perturbed due to the decoupling scheme and that $^{13}C_\beta$ resonances of serines are not sufficiently separated from the $^{13}C_\alpha$ region to allow effective homonuclear decoupling. The original four-band adiabatic decoupling scheme proposed for the HNCA experiment by Wagner and co-workers[33] with individual bands covering the backbone $^{13}C'$, the threonine $^{13}C_\beta$, the main region in which $^{13}C_\beta$ resonate, and finally the alanine $^{13}C_\beta$ region[13] is replaced by a three-band decoupling scheme. The last two regions, the main $^{13}C_\beta$ and the alanine $^{13}C_\beta$ region, respectively, are combined yielding a total bandwidth of approximately 30 ppm. Evolution of $^{13}C_\alpha$ magnetization components due to $^2J(C_\alpha,C_\gamma)$ couplings potentially attenuates the cross and reference peak intensities in an unfavorable manner, the slightly enlarged high-field aliphatic band effectively eliminates these passive couplings. The decoupling field at the high-field end of the $^{13}C_\beta$ chemical shift range with an offset of −3900 Hz, the threonine $^{13}C_\beta$ region with a bandwidth of approximately 6 ppm and a corresponding offset of 2270 Hz, as well as the backbone $^{13}C'$ decoupling field with a bandwidth of approximately 30 ppm and an offset of 18200 Hz are mixed together following the vector addition procedure.[35] Simulations carried out with NMRSim (Bruker Analytik GmbH, Rheinstetten) indicated a moderate increase of approximately 16% for the average RF decoupling field strength required for the three homonuclear decoupling bands with respect to the four-band adiabatic decoupling scheme with separate main $^{13}C_\beta$ and alanine $^{13}C_\beta$ regions published previously.[13] We use adiabatic HS2 inversion pulses,[36,37] flattened versions of the well-known hyperbolic secant pulse,[38] of duration 4 ms with frequency sweeps of 5000 ($^{13}C'$ and aliphatic $^{13}C_\beta$ bands) and 1125 Hz (threonine $^{13}C_\beta$ band), respectively. First, the individual pulses were optimized with respect to an adiabaticity factor of 5[39] usually ensuring 100% inversion of a two-level system by calculating spin-inversion profiles $\langle M_z \rangle$ as a function of $\gamma B_1/2\pi$. The experimental decoupling profile of the three homonuclear decoupling bands with an optimized $\gamma B_1/2\pi^{max} = 6720$ Hz is shown in Figure 2. The recommended adiabaticity factor of 5 for individual adiabatic inversion pulses is too conservative for decoupling schemes where these pulses are

(33) Matsuo, H.; Kupèe, Ç.; Wagner, G. *J. Magn. Reson., Ser. B* **1996**, *113*, 190−194.

(34) Hu, J.-S.; Bax, A. *J. Am. Chem. Soc.* **1996**, *118*, 8170−8171.

(35) Kupče, Ē.; Freeman, R. *J. Magn. Reson., Ser. A* **1993**, *105*, 234−238.

(36) Kupče, Ē.; Freeman, R. *J. Magn. Reson., Ser. A* **1995**, *117*, 246−256.

(37) Tannús, A.; Garwood, M. *J. Magn. Reson., Ser. A* **1996**, *120*, 133−137.

(38) Silver, M. S.; Joseph, R. I.; Hoult, D. I. *J. Magn. Reson.* **1984**, *59*, 347.

(39) Baum, J.; Tycko, R.; Pines, A. *Phys. Rev. A* **1985**, *32*, 3435−3447.

expanded in suitable supercycles. Therefore, we reduced the $\gamma B_1/2\pi^{max}$ of 6720 Hz stepwise down to 4240 Hz and experimentally verified the clean and effective decoupling performance as depicted in Figure 2. Two further effects associated with HS2 homonuclear decoupling require special attention. Bandselective decoupling schemes cause measurable Bloch-Siegert shifts. The employed decoupling scheme leads to downfield Bloch−Siegert shifts of the $^{13}C_\alpha$ resonances because of off-resonance effects from the decoupling field. However, these shifts are rather small, ranging from 0.362 ppm at the high field end (48.25 ppm $^{13}C_\alpha$ resonance frequency) to 0.103 ppm at the low field end (61.25 ppm $^{13}C_\alpha$ resonance frequency) of the $^{13}C_\alpha$ chemical shift range at a proton resonance frequency of 600 MHz, and can be calculated on the basis of known theory.[27] The second effect presented a serious drawback of the homonuclear $^{13}C_\beta$ decoupling as decoupling sidebands are associated with each signal hampering the interpretation of relatively weak cross-peak intensities in close vicinity to the intense reference peaks. These decoupling sidebands are due to modulations of the effective field by the adiabatic inversion pulses during t_2. This gives rise to characteristic sideband patterns at resonance offsets that are multiples of the inverse of the pulse duration. As previously reported by Weigelt et al. we observed a correlation between the intensities of the decoupling sidebands and the employed decoupling field strength, $\gamma B_1/2\pi^{max}$.[40] To scale the sideband intensities to a tolerable level the decoupling field strength was further reduced, finally reaching a $\gamma B_1/2\pi^{max}$ of 3360 Hz (Figure 1, Supporting Information, illustrates the effect of reducing $\gamma B_1/2\pi^{max}$ from 6720 down to 3360 Hz, thereby scaling the relative sideband intensities from 32.8% to 9.5%). Further reduction of the decoupling sidebands at the expense of increased t_1 noise in the indirect ω_2 dimension was achieved by averaging out the modulation of the effective field using asynchronous instead of synchronous homonuclear $^{13}C_\beta$ decoupling as shown in the Supporting Information (Figure 1, Supporting Information). It should be noted that RF power requirements are further reduced for the proposed HN(CO)CA like experiment because only two of the three discussed homonuclear decoupling bands covering the two $^{13}C_\beta$ region are applied while the $^{13}C'$ region is decoupled using shaped bandselective pulses.[33]

Determination of Heteronuclear $^3J(C_\alpha,H^N)$ Coupling Constants. The pulse sequence for the determination of heteronuclear $^3J(C_\alpha,H^N)$ coupling constants is based on the well-known HNCO scheme.[14] All RF pulses on $^{13}C'$ are applied in a bandselective way, G4 Gaussian cascades of duration 409.6 μs were used for excitation, while inversion was achieved using Q3 Gaussian cascades of duration 512 μs.[28] To avoid long-range heteronuclear $^nJ(H^N,C')$ coupling modulation during the acquisition a bandselective $^{13}C'$ decoupling using Q3 inversion pulses of duration 1024 μs expanded according to MLEV-16 was used.[41] The evolution of the uniform one-bond $^1J(C_\alpha,C')$ coupling of 54 Hz leads to a splitting of the cross-peaks in the indirect ω_2 ($^{13}C'$) dimension. Thus, the $^{13}C'_{i-1}$ and $^1H^N_i$ nuclei are correlated without disturbing the passive $^{13}C_{\alpha i-1}$ spin resulting in E.COSY like multiplets corresponding to the α and β spin states of $^{13}C_{\alpha i-1}$ which allows the small $^3J(C_\alpha,H^N)$ couplings to be measured as their displacement in the ω_3 ($^1H^N$) dimension. As discussed before possible underestimation of the vicinal $^3J(C_\alpha,H^N)$ coupling constants due to $^{13}C_\alpha$ spin flips is negligible. The values of the coupling constants have been determined by taking appropriate ω_3 traces, displacing the two extracted traces with respect to each other and forming the integral of the power difference spectrum as a function of the displacement. The coupling constant is determined at the minimum of the integral.[42] This provides a method for the quantitative investigation of vicinal $^3J(C_\alpha,H^N)$ coupling constants in uniformly ^{13}C,^{15}N-labeled proteins in a way that the sensitivity of the experiment is not limited by fast transverse relaxation of $^{13}C_\alpha$ spins.

Applications to Ubiquitin. For each amide, $^1H^N_i$, up to three cross-peaks can be observed in the HN(COCA)CA experiment corresponding to the intense reference peak at the $^{13}C_{\alpha i-1}$ resonance and weaker cross-peaks to neighboring $^{13}C_\alpha$ resonances of residues $i-1\pm1$. For proline and arginine residues further cross-peaks arising from $^3J(C_\alpha,C_\delta)$ correlations can be observed. These unwanted correlations cannot be sufficiently suppressed because their $^{13}C_\delta$ chemical shift range falls well inside the main $^{13}C_\alpha$ region. The quality of the data that we have obtained from the HN(COCA)CA experiment (Figure 1) described above is illustrated in Figure 3. Two distinct small regions extending from Thr22 to Lys29 and Gln41 to Lys48 are shown. ω_2,ω_3 strips are taken at the $^1H^N$,^{15}N frequency of the succeeding residue. The secondary structure elements of the small protein ubiquitin, consisting of 76 residues, are a five-stranded β-sheet, an α- and two 3_{10}-helices. The first region shown in Figure 3 includes residues being part of an α-helical secondary structural element, starting at Ile23, while the second region between Gln41 and Phe45 forms the third strand of the β-sheet followed by a tight turn formed by Ala46 and Gly47 according to the crystal structure.[15] Within the α-helical segment spanning residues Ile23 − Glu34, we cannot observe any visible sequential connectivities due to vicinal $^3J(C_\alpha,C_\alpha)$ couplings. In contrast, strong cross-peaks connecting neighboring $^{13}C_{\alpha i}$ and $^{13}C_{\alpha i\pm1}$ due to $^3J(C_\alpha,C_\alpha)$ couplings in the range of 1.5−1.9 Hz are observable in both the β-sheet as well as the turn region as shown in Figure 3. Table 1 lists the extracted $^3J(C_\alpha,C_\alpha)$ and $^3J(C_\alpha,H^N)$ coupling constant values determined from experiments presented above for the residues illustrated in Figure 3 in combination with corresponding ψ_{i-1} and ω_i backbone torsion angles obtained from the crystal structure of ubiquitin. The lack of interpretable cross-peak intensities to neighboring $^{13}C_\alpha$ resonances of residues $i\pm1$ in the α-helical segment can neither be explained on the basis of varying ω torsion angles (Figure 2, Supporting Information) nor on the basis of the overall lower sensitivity of the employed pulse scheme in this region (Figure 3, Supporting Information). All peptide bonds in

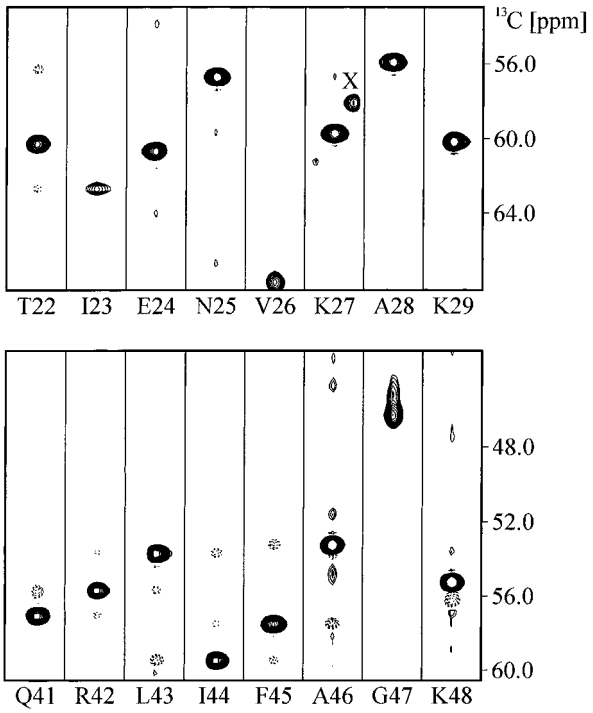

Figure 3. (ω_1, ω_3) strips from the HN(COCA)CA experiment of perdeuterated ubiquitin, taken at the $^1H^N$ (ω_3) and ^{15}N (ω_1) frequencies of Ile23, Glu24, Asn25, Val26, Lys27, Ala28, and Lys29 for the first region and Arg42, Leu43, Ile44, Phe45, Ala46, Gly47, Lys48, and Gln49 for the second region, respectively. Correlations due to sequential $^3J(C_\alpha,C_\alpha)$ coupling constants are negative (dashed contours). Positions from residues with $^1H^N$ (ω_3) and ^{15}N (ω_1) chemical shifts in the vicinity of the selected amide strip are marked X. The relatively weak reference peak intensity of Ile23 is due to exchange broadening of the succeeding Glu24 amide. The Gly47 $^{13}C_\alpha$ resonance is perturbed due to the main $^{13}C_\beta$ decoupling band. The employed HS2 decoupling scheme provide clean and efficient decoupling for the main $^{13}C_\alpha$ region, almost effective homonuclear decoupling combined with moderate spectral distortion is achieved at the low-field end of the $^{13}C_\alpha$ region as can be verified by inspection of residue Val26 with $\delta(^{13}C_\alpha) = 66.95$ ppm.

(40) Weigelt, J.; Hammarström, A.; Bermel, W.; Otting, G. *J. Magn. Reson., Ser. B* **1996**, *110*, 219−224.
(41) Levitt, M. H.; Freeman, R.; Frenkiel, T. *J. Magn. Reson.* **1982**, *47*, 308−320.
(42) Schwalbe, H.; Rexroth, A.; Eggenberger, U.; Geppert, T.; Griesinger, C. *J. Am. Chem. Soc.* **1993**, *115*, 7878−7879.

Table 1. Values of Extracted $^3J(C_\alpha,C_\alpha)$ and $^3J(C_\alpha,H^N)$ Coupling Constants for the Ubiquitin Residues Illustrated in Figure 3

residue	$^3J(C_\alpha,C_\alpha)$ [Hz][a]	rmsd [Hz][b]	$^3J(C_\alpha,H^N)$ [Hz][c]	ϕ_{i-1} [°][d]	ω_I [°][d]
Thr22	1.62	0.16	0.65	148.4	−178.7
Ile23	1.60		0.43	160.4	176.6
Glu24	<1.0		0.03	−37.2	176.1
Asn25	<0.9		0.11	−40.5	178.4
Val26	n.d.[e]		0.16	−44.4	177.7
Lys27	<0.9		0.21	−46.4	−178.7
Ala28	<0.9		0.24	−38.0	174.4
Lys29	<0.8		0.11	−38.1	177.4
Gln41	n.d.[e]		0.27	−10.5	−176.0
Arg42	1.75		0.84	129.7	−178.9
Leu43	1.52	0.12	0.79	116.0	178.2
Ile44	1.86	0.06	0.92	130.2	177.7
Phe45	1.53	0.04	0.75	131.8	179.1
Ala46	1.76	0.11	0.65	129.6	172.8
Gly47	n.d.[e]		0.27	46.0	177.9
Lys48	n.d.[e]		0.54	21.6	−179.6

[a] Values of $^3J(C_\alpha,C_\alpha)$ were determined from the ratio of reference and the cross-peak intensities as described in the text. [b] Pairwise root-mean-square (rms) difference of $^3J(C_\alpha,C_\alpha)$ coupling constant values measured twice, once starting from $^{13}C_{\alpha i}$ and detection of the cross-peak intensity at the frequency of $^{13}C_{\alpha i-1}$, and once vice versa. [c] Values of $^3J(C_\alpha,H^N)$ coupling constants have been determined by taking appropriate ω_3 traces, displacing the two extracted traces with respect to each other and forming the integral of the power difference spectrum as a function of the displacement as described in the text. [d] Values of corresponding ψ_{i-1} and ω_i backbone torsion angles are obtained from the crystal structure of ubiquitin. [e] $^3J(C_\alpha,C_\alpha)$ of residue Gln41 cannot be determined because of spectral overlap. Upper limits of $^3J(C_\alpha,C_\alpha)$ of residue Val26 are not given because the downfield $^{13}C_\alpha$ reference resonance is slightly perturbed by the threonine $^{13}C_\beta$ decoupling band and the corresponding cross-peaks are not observable. Values of $^3J(C_\alpha,C_\alpha)$ of residues Gly47 and Lys48 not possible to determine because high-field $^{13}C_\alpha$ resonance are perturbed due to the main $^{13}C_\beta$ decoupling band. Maximum values of unobserved $^3J(C_\alpha,C_\alpha)$ couplings are determined from the intensity ratio of the smallest cross-peak observable and the corresponding reference intensity. Coupling constant values are not corrected for $^{13}C_\alpha$ spin flips.

ubiquitin are in the preferred *trans* conformation. As a consequence of the partial double bond character, variations of ω fall in the range $\pm10°$. All measured values of vicinal $^3J(C_\alpha,C_\alpha)$ couplings associated with the intervening backbone torsion angle ω are shown in Figure 4 in combination with the neighboring ψ_{i-1} torsion angle as a function of the sequence. Surprisingly, the distribution of determined vicinal $^3J(C_\alpha,C_\alpha)$ coupling constants is non-uniform in contrast to what one would expect from small variations of the intervening torsion angle ω. Out of 40 coupling constant values measured the minimum value was found for Thr9, Asn60, and Ile61, $^3J(C_\alpha,C_\alpha) = 1.1$ Hz. The maximum value corresponds to the N-terminal residue Gln2 and equals 2.2 Hz. The relatively small standard deviation of the mean coupling constant, $\langle^3J(C_\alpha,C_\alpha)\rangle = 1.65$ Hz $\pm$ 0.2 Hz, reflects the fact of absent cross-peaks in regions identified on the basis of their ϕ,ψ backbone torsion angles as α- or 3_{10}-helices. According to the crystal structure, residues Ile23-Glu34 span an α-helical segment, two short 3_{10}-helices are formed by residues Pro38-Gln40 and Ser57-Tyr59, respectively. None of these residues shows sequential cross-peaks. Residues Leu8 to Lys11 span a tight turn connecting the first and the second of the five-stranded β-sheet, the preceding Leu8 has a crystallographic ψ value of $-6.9°$. The coupling constant determined for Asn60 and Ile61 is 1.1 Hz. Both residues are located in a coil region with the preceding Tyr59 (crystallographic $\psi = 4.7°$) being part of the second 3_{10}-helix. There exists a striking correlation of the vicinal $^3J(C_\alpha,C_\alpha)$ couplings with the neighboring backbone torsion angle ψ_{i-1}. Regular secondary structure elements show a strong dependence on the backbone torsion angle ψ with most populated angles of $\psi = -39.8°$ ($\pm12.2°$) for α-helices, $\psi = -16.5°$ ($\pm$ 34.7°) for 3_{10}-helices and $\psi = 123.0°$ ($\pm$ 60.0°) for β-sheets as obtained from a database of 85 of the highest-resolution crystal structures.[16] The property of a residue to exhibit a measurable $^3J(C_\alpha,C_\alpha)$ coupling constant clearly correlates with the ψ_{i-1} angle but not with the value of ϕ_i. Thus $^3J(C_\alpha,C_\alpha)$ couplings enable the ψ torsion

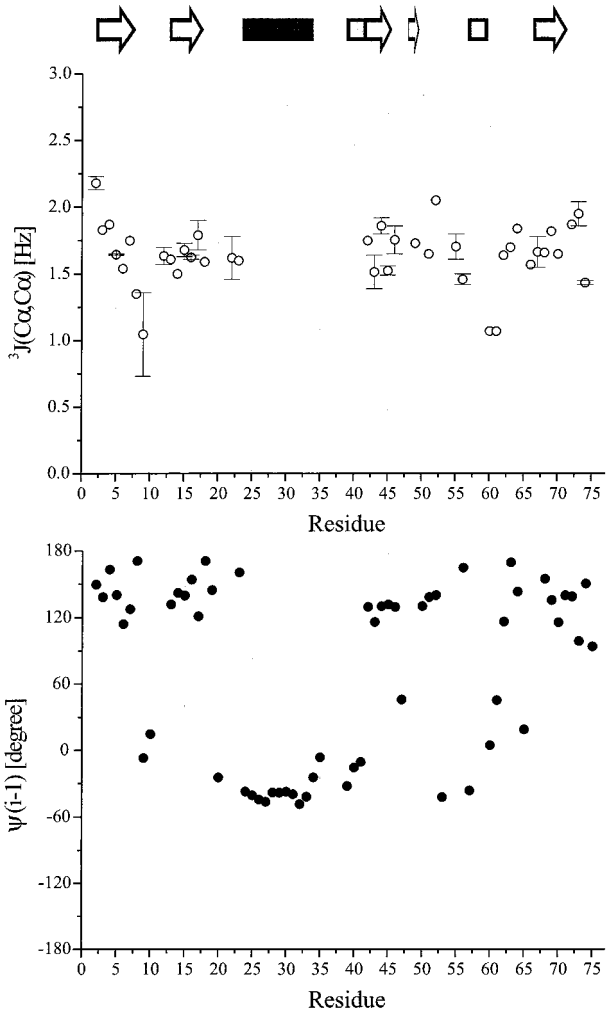

Figure 4. $^3J(C_\alpha,C_\alpha)$ (open circles) coupling constants measured in the HN(COCA)CA experiment for ubiquitin along the sequence combined with ψ_{i-1} (filled circles) taken from the crystal structures. Pairwise root-mean-square (rms) difference of $^3J(C_\alpha,C_\alpha)$ coupling constant values which could be measured twice, once starting from $^{13}C_{\alpha i}$ and detection of the cross-peak intensity at the frequency of $^{13}C_{\alpha i-1}$, and once vice versa are given as error bars. Missing coupling constant values are either in regions identified on the basis of their ϕ,ψ backbone torsion angles as α- or 3_{10}-helices, glycine $^{13}C_\alpha$ resonances and succeeding residues, where peak intensities are perturbed due to the main $^{13}C_\beta$ decoupling band or $^{13}C_\beta$ resonances and succeeding resonances of serines which are not sufficiently separated from the $^{13}C_\alpha$ region to allow effective homonuclear decoupling. Ubiquitin's secondary structure elements as determined by the program MOLMOL[63] are shown on the top (arrow: β-sheet; black bar: α-helix; gray bar: 3_{10}-helix).

angle to be probed in a qualitative manner by distinguishing positive (β-sheet conformations) and negative ψ values (α- or 3_{10}-helical conformations) from simple visual inspection which may prove to be of particular importance for structural studies of perdeuterated proteins in solution. Vicinal $^3J(N,C_\beta)$ couplings are of vanishing magnitude and $^3J(N,H_\alpha)$ are not measurable due to substitution of ^1H by ^2H. Furthermore, $^3J(N,N)$ homonuclear couplings show a considerable spread of measured values for very similar associated torsion angles ψ not consistent with the classical Karplus-type relationship with small variations between 0.14 and 0.36 Hz for residues in β-sheet conformations and below 0.15 Hz for residues in α-helical segments.[43] Consequently, vicinal coupling constants involving the ^{15}N nucleus are not well suited in restricting the ψ conformational space in perdeuterated proteins. Recently proposed elegant approaches for this purpose relying

(43) Theis, K.; Dingley, A. J.; Hoffmann, A.; Omichinski, J. G.; Grzesiek, S. *J. Biomol. NMR* **1997**, *10*, 403−408.

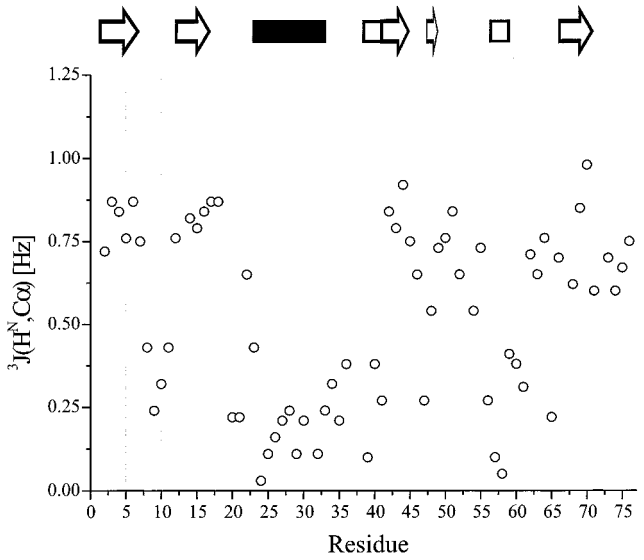

Figure 5. $^3J(C_\alpha,H^N)$ (open circles) coupling constants measured in the HNCO[C_α] experiment for ubiquitin along the sequence of ubiquitin. Ubiquitin's secondary structure elements as determined by the program MOLMOL[63] are shown on the top (arrow: β-sheet; black bar: α-helix; gray bar: 3_{10}-helix).

on cross-correlated dipole−dipole[44] or dipole-CSA[45] rates involve $^1H_\alpha$−$^{13}C_\alpha$ dipolar interactions and therefore fail in perdeuterated proteins.

Inspired by the valuable dependence of vicinal homonuclear $^3J(C_\alpha,C_\alpha)$ coupling constants we attempt to measure the complementary vicinal heteronuclear $^3J(C_\alpha,H^N)$ coupling constants. Because all vicinal couplings between $^{13}C_\alpha$ and $^1H^N$ nuclei adopting a *cis* orientation are quite small, they are most easily measured using an E.COSY-type experiment. As observed for the $^3J(C_\alpha,C_\alpha)$ couplings the distribution of determined vicinal $^3J(C_\alpha,H^N)$ coupling constants using the E.COSY-type HNCO[C_α] experiment is nonuniform. Numerical values for the selected residues shown in Figure 3, namely Ile23, Glu24, Asn25, Val26, Lys27, Ala28, and Lys29 for the first region and Arg42, Leu43, Ile44, Phe45, Ala46, Gly47, Lys48, and Gln49 for the second region, respectively, are given in Table 1. All measured values of vicinal $^3J(C_\alpha,H^N)$ coupling constants are shown in Figure 5 as a function of the sequence of ubiquitin. The displacement vectors $\mathbf{J}_{C\alpha}$ indicate uniform signs for all determined $^3J(C_\alpha,H^N)$ coupling constant values in ubiquitin. Although smaller in magnitude with respect to the homonuclear $^3J(C_\alpha,C_\alpha)$ couplings due to the *cis* orientation of involved $^{13}C_\alpha$ and $^1H^N$ nuclei, significant variations of $^3J(C_\alpha,H^N)$ coupling constant values clustering in distinct ranges are observable for ubiquitin. The mean value of $\langle^3J(C_\alpha,H^N)\rangle$ is 0.52 Hz ± 0.28 Hz and it ranges from 0.03 to 0.98 Hz. The $^3J(C_\alpha,H^N)$ coupling constant values in ubiquitin, where all peptide bonds are in the *trans* conformation, follow the same trends observed for homonuclear $^3J(C_\alpha,C_\alpha)$ couplings. The variation cannot be explained on the basis of variations of the intervening torsion angle ω. Smaller values of approximately 0.20 Hz are observed for α-helical secondary structure elements, whereas larger values, ∼0.80 Hz, of $^3J(C_\alpha,H^N)$ couplings are found for β-sheet conformations. It should be mentioned, that the actual torsion angle between the two coupled nuclei $^1H_i^N$ and $^{13}C_{\alpha i-1}$ is not directly ω but a phase shift of approximately 180° depending on the trigonal geometry of the nitrogen substituents has to be incorporated. This particular coupling should therefore be sensitive to distortions from planarity of the peptide bond.

Quantitative Description of $^3J(C_\alpha,H^N)$ Couplings. To a first approximation we fitted the data according to $f[^3J(C_\alpha,H^N),\psi_{i-1}]$, yielding a correlation coefficient R for the least-squares linear fit of 0.84, as illustrated in Figure 6. The $^3J(C_\alpha,H^N)$ coupling constant values based on this empirically derived linear relation for α-helices ($\psi = -39.6°$)

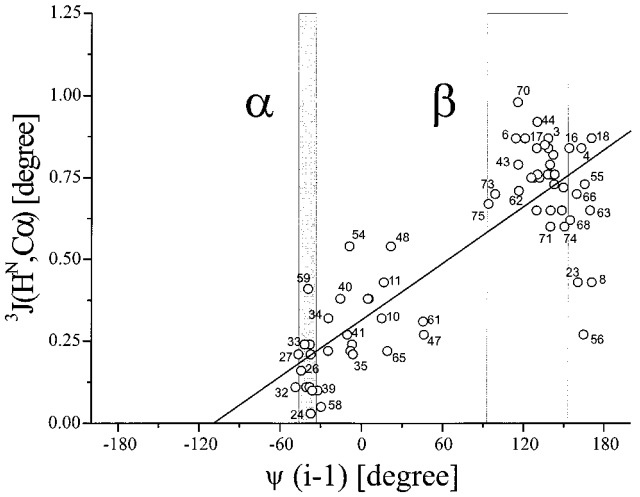

Figure 6. $^3J(C_\alpha,H^N)$ (open circles) coupling constants measured in the HNCO[Cα] experiment for residues in ubiquitin as a function of crystallographic ψ_{i-1} torsion angles. The correlation coefficient R for the least-squares linear fit is 0.84. The intercept for $\psi_{i-1} = 0°$ is $^3J(C_\alpha,H^N) = 0.315$ Hz while the slope is 2.884×10^{-3} [Hz/°]. Typically populated α-helical regions (dark gray box) with a corresponding mean torsion angle $\psi_{i-1} = -39.8 \pm 12.2°$ and β-sheet regions (light gray box) with a corresponding mean torsion angle $\psi_{i-1} = 123.0 \pm 60.0°$ as obtained from a statistical analysis of a protein database are highlighted.[16]

and for β-sheets ($\psi = 123.1°$) are 0.20 and 0.67 Hz, respectively. This reflects a similar qualitative correlation between experimentally derived $^3J(C_\alpha,H^N)$ and crystallographic ψ_{i-1} backbone torsion angles making these particular couplings potentially useful in restricting the ψ conformational space in polypeptides.

The presented results are among the first where vicinal ^3J coupling constants depend primarily on adjacent torsion angles. Theoretical studies on ^3J coupling constants have shown that the general features of the simple Karplus relation are potentially complicated by a number of factors. Other mechanisms besides Fermi contact contributions, bond angles, substituents and neighboring torsion angles might actually contribute.[46−49] Therefore, Edison et al. suggested the fitting of coupling constant data to two-dimensional surfaces accounting for contributions of varying ϕ_i and ψ_i torsion angles.[46,50] The aim of the following section is to provide a framework for possible theoretical analysis of the experimentally observed $^3J(C_\alpha,H^N)$ coupling constant variations. Most likely, the ϕ_i torsion angle is a candidate to influence the $^3J(C_\alpha,H^N)$ coupling constant values in addition to variations in torsion angles ψ_{i-1} due to the strong correlation of ϕ_i,ψ_i defining the conformation of the polypeptide chain. Accounting for ϕ_i torsion angle contributions, to a first approximation a linear correlation $f[^3J(C_\alpha,H^N),\phi_i]$ with a negative slope can be established. Data from residues Gly10, 35, 47, 75, 76, and interestingly, Ala46, Asn60, and Glu64, were neglected as shown in Figure 7. Although the correlation coefficient R for the least-squares linear fit is only −0.71, the probability P that this correlation occurs by chance is negligible ($P < 10^{-4}$). Glycine residues, that have no C_β atom attached to the C_α atom, frequently populate otherwise disfavored regions of the Ramachandran plot with positive ϕ values. All glycines in ubiquitin where vicinal $^3J(C_\alpha,H^N)$ couplings could be measured are in coil regions, adopting positive ϕ values. This is also true for residues Ala46, Asn60 and Glu64. However, similar deviations from the linear relation $f[^3J(C_\alpha,H^N),\psi_{i-1}]$ were not observed for these three nonglycine residues. $^3J(C_\alpha,H^N)$ coupling constant values derived from the empirical

(44) Reif, B.; Hennig, M.; Griesinger, C. *Science* **1997**, *276*, 1230−1233.
(45) Yang, D.; Konrat, R.; Kay, L. E. *J. Am. Chem. Soc.* **1997**, *119*, 11938−11940.
(46) Edison, A. S.; Markley, J. L.; Weinhold, F. *J. Biomol. NMR* **1994**, *4*, 519−542.
(47) Edison, A. S.; Markley, J. L.; Weinhold, F. *J. Phys. Chem.* **1993**, *97*, 11657−11665.
(48) Head-Gordon, T.; Head-Gordon, M.; Frisch, M. J.; Brooks, C. L., III; Pople, J. A. *J. Am. Chem. Soc.* **1991**, *113*, 5989−5997.
(49) Barfield, M.; Grant, D. M. *Adv. Magn. Reson.* **1965**, *1*, 149−193.
(50) Edison, A. S.; Markley, J. L.; Weinhold, F. *J. Biomol. NMR* **1994**, *4*, 543−551.

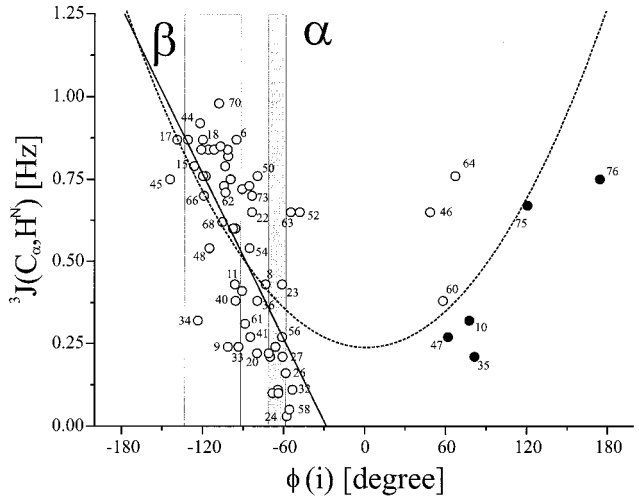

Figure 7. $^3J(C_\alpha,H^N)$ coupling constants measured in the HNCO[Cα] experiment for residues in ubiquitin as a function of crystallographic ϕ_i torsion angles. The correlation coefficient R for residues depicted as open circles for the least-squares linear fit is −0.71. The intercept for $\phi_i = 0°$ is $^3J(C_\alpha,H^N) = -0.236$ Hz, while the slope is -8.348×10^{-3} [Hz/°] (solid line). The statistical significance of the quadratic relation between all measured $^3J(C_\alpha,H^N)$ couplings (open and filled circles) and ϕ_i, $f[^3J(C_\alpha,H^N),\phi_i] = A + D \times (\phi_i)^2$, is described by the correlation coefficient $R = 0.62$. Coefficients are $A = 0.2335$ Hz and $D = 3.254 \times 10^{-5}$ [Hz/°^{2}] (dashed line). Typically populated α-helical regions (dark gray box) with a corresponding mean torsion angle $\phi_i = -64.7 \pm 12.8°$ and β-sheet regions (light gray box) with a corresponding mean torsion angle $\phi_i = -112.6 \pm 41.4°$ as obtained from a statistical analysis of a protein database are highlighted.[16] Residues shown as filled circles (Gly10, 35, 47, 75, 76), as well as Ala46, Asn60, and Glu64 were neglected in the linear fit.

linear relation based on residues with negative ϕ torsion angles for the secondary structure elements typically found in proteins are 0.30 Hz (α-helices, $\phi = -64.1°$) and 0.71 Hz (β-sheets, $\phi = -113.1°$), respectively. All measured $^3J(C_\alpha,H^N)$ couplings fit a quadratic relation, $f[^3J(C_\alpha,H^N),\phi_i] = A + D \times (\phi_i)^2$, with a correlation coefficient R for the least-squares fit of 0.62. The resulting curve is shown in Figure 7 together with the linear relation obtained neglecting residues with positive ϕ_i torsion angles. Again, the probability P that this nonlinear correlation results from random uncertainties is negligible ($P < 10^{-4}$).

We fitted the experimentally determined vicinal $^3J(C_\alpha,H^N)$ couplings to the two-dimensional ϕ,ψ surface of the crystal structure. A similar analysis fitting the experimentally derived homonuclear $^3J(C_\alpha,C_\alpha)$ couplings to the crystallographic $[\phi_i,\psi_{i-1}]$ surface was not carried out due to the lack of data in many regions of the ϕ_i,ψ_{i-1} space. By applying the proposed quantitative J correlation HN(COCA)CA pulse scheme only upper limits for $^3J(C_\alpha,C_\alpha)$ couplings in helical conformations can be obtained. Coil regions with positive ϕ torsion angels are most frequently populated by glycine residues, thus only very limited experimental $^3J(C_\alpha,C_\alpha)$ coupling constant data are measurable.

The experimental coupling constant data for all residues in ubiquitin, where vicinal $^3J(C_\alpha,H^N)$ couplings could be determined, fit an equation of the type:

$$f[\phi_i,\psi_{i-1}] = A + B \times \phi_i + C \times \psi_{i-1} \quad (1)$$

defining a plane with coefficients $A = 0.2854$ Hz, $B = -4.867 \times 10^{-4}$ [Hz/°] and $C = 2.822 \times 10^{-3}$ [Hz/°]. The correlation coefficient R for the least-squares linear fit is 0.85. The rmsd between measured $^3J(C_\alpha,H^N)$ couplings and those predicted by eq 1 is 0.14 Hz.

The statistical significance, weather multi-dimensional models with more adjustable parameters actually better represent the experimental data, can be tested using an F-statistic defined as:[51,52]

$$F = \nu_2 (\chi_1 - \chi_2)/(\nu_2 - \nu_1) \chi_2 \quad (2)$$

where χ_1 and χ_2 are the sum of squared errors between experimental and predicted parameters for two models with ν_1 and ν_2 statistical degrees of freedom ($\nu_2 > \nu_1$). The statistical degree of freedom for a certain model, $\nu = N - n$, is the difference between the independently measured number of data points N (here assumed to be the number of residues) and the number of parameters n in the associated fitting function f. Large values for F according to eq 2 correspond to significant improvement of the fit as opposed to random statistical reduction of the χ values due to the incorporation of additional parameters. The derived values of the F-statistics, calculated from the χ_i sum of squared errors of the fits to the experimental data, are compared with the tabulated $P = 0.01$ critical values. The integral probability value $P = 0.01$ characterizes the probability greater or equal to 99% of observing the corresponding F value from a random data set with ν_1,ν_2 degrees of freedom.[53]

To evaluate, if the added ϕ_i dependence in eq 1 better represents the experimental data in a statistically significant manner relative to the linear fit $f[^3J(C_\alpha,H^N),\psi_{i-1}]$, we calculated the F-statistic according to eq 2. The calculated value, $F = 2.88$, is smaller than the corresponding critical value for an exact F-distribution, $F_{0.01,1,65} = 7.04$. Thus, the ϕ_i related coefficient B in eq 1 does not statistically deviate from zero and must not be included in the model.

However, as a ϕ_i dependence of the measured couplings is evident in the correlations $f[^3J(C_\alpha,H^N),\phi_i]$ shown in Figure 7, although less pronounced than the ψ_{i-1} dependence, different models were tested to resolve statistically significant ϕ_i related coefficients. The experimental $^3J(C_\alpha,H^N)$ coupling constant data for all residues in ubiquitin fit a polynomial equation of the type:

$$f[\phi_i,\psi_{i-1}] = A + C \times \psi_{i-1} + D \times (\phi_i)^2 \quad (3)$$

with coefficients $A = 0.1972$ Hz, $C = 2.426 \times 10^{-3}$ [Hz/°] and $D = 1.691 \times 10^{-5}$ [Hz/(°)^2]. The correlation coefficient R for the least-squares linear fit is 0.89. Applying the F-statistic results in F = 21.62 with respect to the linear fit $f[^3J(C_\alpha,H^N),\psi_{i-1}]$ with the corresponding critical value for an exact F-distribution being $F_{0.01,1,65} = 7.04$. This large F value fulfills the condition, $F > F_{0.01,1,65}$, thus justifying the inclusion of the additional parameter D in the fitting function. The surface defined by eq 3 is shown in Figure 8a together with the experimentally derived vicinal $^3J(C_\alpha,H^N)$ couplings. The rmsd between measured $^3J(C_\alpha,H^N)$ couplings and those predicted by eq 3 is 0.12 Hz. (Table 2, Supporting Information). A correlation plot between the experimentally observed $^3J(C_\alpha,H^N)$ coupling constant and those values predicted on the basis of eq 3 using neighboring ψ_{i-1} and ϕ_i torsion angle from the 1.8 Å X-ray crystal structure of ubiquitin is shown in Figure 9a.

Additionally, following Edison et al.,[46] the 67 vicinal $^3J(C_\alpha,H^N)$ couplings derived from the HNCO[C_α] experiment were fitted to Fourier series:

$$f[\phi_i,\psi_{i-1}] = \Sigma_q^m \Sigma_p^n \{\cos(q \times \phi_i) \cos(p \times \psi_{i-1}) + \cos(q \times \phi_i) \sin(p \times \psi_{i-1}) + \sin(q \times \phi_i) \cos(p \times \psi_{i-1}) + \sin(q \times \phi_i) \sin(p \times \psi_{i-1})\} \quad (4)$$

by least-squares minimization of $f[\phi_i,\psi_{i-1}]$ to first-order fit ($m = n = 1$). The correlation coefficient R for this fitting procedure applying 9 coefficients was 0.93. The evaluation of the statistical significance of adding 7 parameters in the Fourier series relative to the linear fit $f[^3J(C_\alpha,H^N),\psi_{i-1}]$ according to the F-statistic yields $F = 10.53$. Again, this value is greater than the appropriate critical value $F_{0.01,7,60} = 2.95$, justifying the added parameters in the model. Coefficients derived from fitting the experimental coupling constant data by first-order two-dimensional Fourier analysis as a function of the neighboring ψ_{i-1} and ϕ_i torsion angles are summarized in Table 2. The 9 Fourier coefficients

(51) Mandel, A. M.; Akke, M.; Palmer, A. G., III. *J. Mol. Biol.* **1995**, *246*, 144−163.

(52) Bevington, P. R. *Data Reduction and Error Analysis for the Physical Sciences*; McGraw-Hill: New York, 1969, 195−203.

(53) Bronstein, I. N.; Semendjajew, K. A. *Taschenbuch der Mathematik*, 24th ed.; Verlag Harri Deutsch: Thun & Frankfurt/M., 1989; pp 24−27.

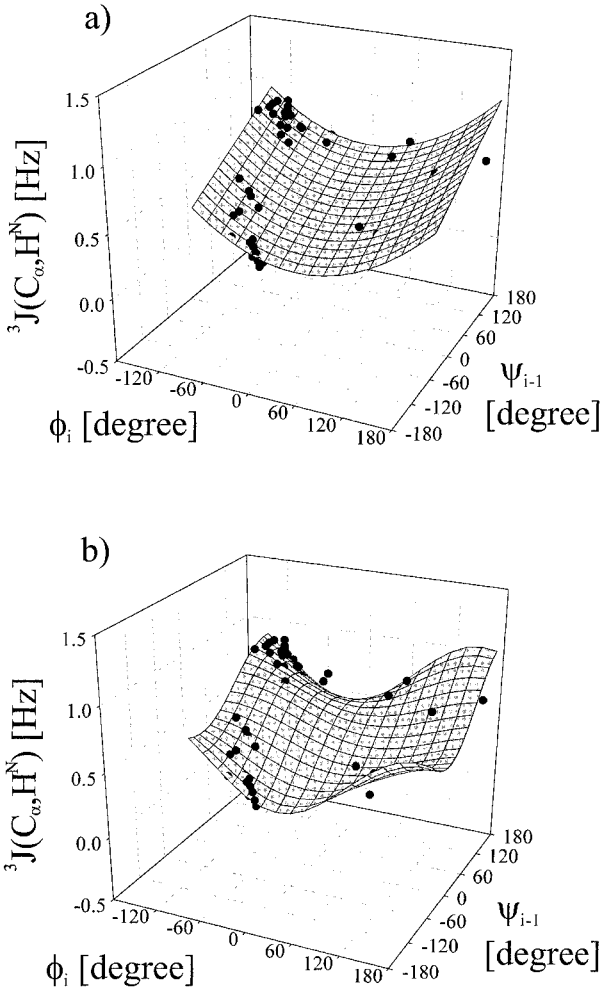

Figure 8. $^3J(C_\alpha,H^N)$ coupling constants (filled circles) measured in the HNCO[Cα] experiment for residues in ubiquitin as a function of the neighboring crystallographic ϕ_i and ψ_{i-1} torsion angles. The experimental coupling constant values were fitted to (a) the three-parameter polynomial eq 3 and (b) a 2D Fourier series using eq 4 to first order ($m = n = 1$) giving rise to the depicted surfaces. The individual Fourier coefficients are summarized in Table 2. The correlation coefficients R for the least-squares linear fits are 0.89 for the polynomial and 0.93 for the Fourier model, respectively.

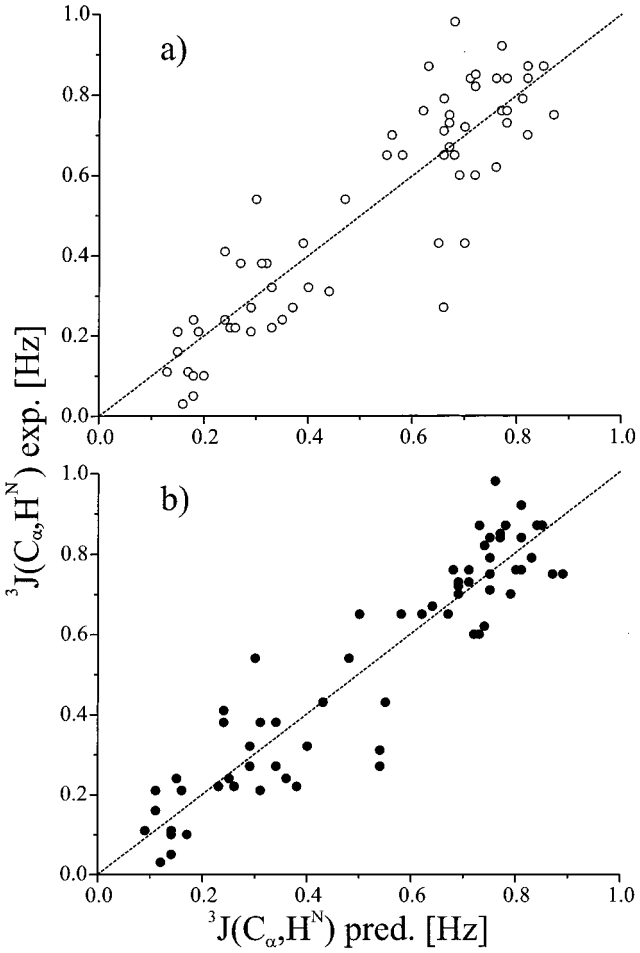

Figure 9. Correlation of the experimental $^3J(C_\alpha,H^N)$ coupling constant values measured in the HNCO[C_α] experiment and values predicted (a) the three-parameter polynomial eq 3 and b) by eq 4 (2D Fourier series to first order ($m = n = 1$)) using neighboring crystallographic ϕ_i and ψ_{i-1} torsion angles of ubiquitin. The correlation coefficients R are (a) 0.89 and (b) 0.93, respectively.

of the first-order analysis give rise to a surface that is shown in Figure 8b together with the experimentally derived vicinal $^3J(C_\alpha,H^N)$ couplings. The rmsd between the experimentally derived vicinal $^3J(C_\alpha,H^N)$ couplings and those predicted using eq 4 to first-order is 0.1 Hz (Table 2, Supporting Information). This correlation is shown in Figure 9b.

Our results indicate that reasonable estimates of the ψ and ϕ torsion angles for ubiquitin allowing the differentiation of typical secondary structural elements are available from one vicinal coupling, $^3J(C_\alpha,H^N)$, in conjunction with the presented empirical relations provided that the conformation of the peptide bond involved is *trans*. The three-parameter polynomial fit as defined in eq 3 is the simplest model adequately describing the experimental $^3J(C_\alpha,H^N)$ couplings in terms of neighboring ψ_{i-1} and ϕ_i torsion angles.

The E.COSY-type method proposed for the measurement of vicinal $^3J(C_\alpha,H^N)$ couplings is straightforward and can be easily carried out in a sensitive way in uniformly ^{13}C,^{15}N enriched protein samples as well.

Conclusions

The backbone torsion angle ω in proteins is to a good approximation restricted to *trans* ($\omega \approx 180°$) or *cis* ($\omega \approx 0°$) orientations of adjacent $C_{\alpha i-1}$- and $C_{\alpha i}$-atoms due to the partial double bond character of the peptide bond. The experimentally observed considerable spread of associated vicinal coupling constants such as $^3J(C_\alpha,C_\alpha)$ or $^3J(C_\alpha,H^N)$ cannot be explained

Table 2. Fourier Coefficients Obtained from Fitting Experimentally Derived Values of $^3J(C_\alpha,H^N)$ Coupling Constants for Ubiquitin by First-Order 2D Fourier Analysis as a Function of Crystallographic ψ_{i-1} and ϕ_i Torsion Angles[a]

coefficient	first-order Fourier analysis [Hz]
constant	0.5390
$\cos(\phi_i)$	−0.2280
$\cos(\psi_{i-1})$	−0.2026
$\sin(\phi_i)$	0.0680
$\sin(\psi_{i-1})$	0.0802
$\cos(\phi_i)\cos(\psi_{i-1})$	0.0664
$\cos(\phi_i)\sin(\psi_{i-1})$	0.1209
$\sin(\phi_i)\cos(\psi_{i-1})$	−0.0798
$\sin(\phi_i)\sin(\psi_{i-1})$	−0.1367

[a] The vicinal $^3J(C_\alpha,H^N)$ couplings derived from the HNCO[C_α] experiment were fitted to two-dimensional Fourier series

$$f[\phi_i,\psi_{i-1}] = \Sigma_q^m \Sigma_p^n \{\cos(q \times \phi_i)\cos(p \times \psi_{i-1}) + \cos(q \times \phi_i)\sin(p \times \psi_{i-1}) + \sin(q \times \phi_i)\cos(p \times \psi_{i-1}) + \sin(q \times \phi_i)\sin(p \times \psi_{i-1})\}$$

by least-squares minimization of $f[\phi_i,\psi_{i-1}]$ to first-order fit ($m = n = 1$). The correlation coefficient R for the fitting procedure applying 9 coefficients was 0.93.

on the basis of varying ω torsion angles but show valuable correlations with the neighboring ψ_{i-1} torsion angle which is usually ill-defined using vicinal coupling constants and not accessible at all in perdeuterated proteins using either scalar or cross correlated relaxation interactions involving the $^1H_\alpha$. Both vicinal couplings therefore provide unique information for the evaluation of protein backbone torsion angles and complement information available from secondary ^{13}C chemical shifts.[54,55] The homonuclear scalar interaction between adjacent $^{13}C_\alpha$ nuclei has never been quantified in proteins so far and can be potentially useful in the sequential assignment process of perdeuterated protein adopting mainly β-sheet conformations. Deviations from a Karplus-type relation have been reported for vicinal coupling constants involving two scalar coupled heavy atoms such as ^{15}N or ^{13}C in proteins. The present study reveals significant contributions from the adjacent ψ_{i-1} and ϕ_i torsion angle for vicinal $^3J(C_\alpha,H^N)$ coupling constants related to the torsion angle ω_i and thereby provides new information with regard to the electron distribution of peptide units**.** The experimental schemes described above are easy to implement and their sensitivity for the investigation of large perdeuterated proteins could, if required, be further improved utilizing the TROSY approach for the $^1H^N-^{15}N$ spin pair.[56,57] and hold the promise to be helpful in their secondary structure elucidation.

Acknowledgment. Dedicated to Professor Horst Kessler on the occasion of his 60th birthday. The Fonds der Chemischen Industrie, the DFG (Gr 1211/4), and the MPG supported this work. M.H. acknowledges a Ph.D. Fellowship by the Fonds der Chemischen Industrie and from the Human Frontier Science Program. H.S. acknowledges support by the Large Scale Facility for Biomolecular NMR at the University of Frankfurt (ERB CT 95 00 34) and from the Department of Chemistry at the Massachusetts Institute of Technology. The authors thank Dr. T. Carlomagno (University of Frankfurt) for many valuable and stimulating discussions. We thank Tracy Handel, Department of Molecular and Cell Biology, University of California, Berkeley, CA, 94720, for the generous gift of $^{13}C,^{15}N$-labeled human ubiquitin.

Supporting Information Available: Three Figures, showing the experimental performance of synchronous HS2 homonuclear decoupling of ^{13}C with varying decoupling RF amplitude $(\gamma B_1/2\pi)^{max}$, variation of the backbone torsion angle ω along the sequence taken from the crystal structure of ubiquitin, and normalized reference peak intensities of the quantitative HN-(COCA)CA experiment. Tables summarizing homonuclear $^3J(C_\alpha,C_\alpha)$ and heteronuclear $^3J(C_\alpha,H^N)$ coupling constant values determined for human ubiquitin (PDF). This material is available free of charge via the Internet at http://pubs.acs.org.

JA9928834

(54) Spera, S.; Bax, A. *J. Am. Chem. Soc.* **1991**, *113*, 5491−5492.
(55) Wishart, D. S.; Sykes, B. D. *J. Biomol. NMR* **1994**, *4*, 171−180.
(56) Pervushin, K.; Riek, R.; Wider, G.; Wüthrich, K. *Proc. Natl. Acad. Sci. U.S.A.* **1998**, *94*, 12366−12371.
(57) Salzmann, M.; Pervushin, K.; Wider, G.; Senn, H.; Wüthrich, K. *Proc. Natl. Acad. Sci. U.S.A.* **1998**, *95*, 13585−13590.
(58) Shaka, A. J.; Keeler, J.; Frenkiel, T.; Freeman, R. *J. Magn. Reson.* **1983**, *52*, 335−338.
(59) Shaka, A. J.; Barker, P. B.; Freeman, R. *J. Magn. Reson.* **1985**, *64*, 547−552.
(60) Boyd, J.; Soffe, N. *J. Magn. Reson.* **1989**, *85*, 406−413.
(61) Tycko, R.; Pines, A.; Gluckenheimer, R. *J. Chem. Phys.* **1985**, *83*, 2775−2802.
(62) Levitt, M. H.; Freeman, R. *J. Magn. Reson.* **1981**, *43*, 502.
(63) Koradi, R.; Billeter, M.; Wüthrich, K. *J. Mol. Graphics* **1996**, *14*, 52−55.